eLIFE
elifesciences.org

Figures and figure supplements

Structural basis for the prion-like MAVS filaments in antiviral innate immunity

Hui Xu, et al.

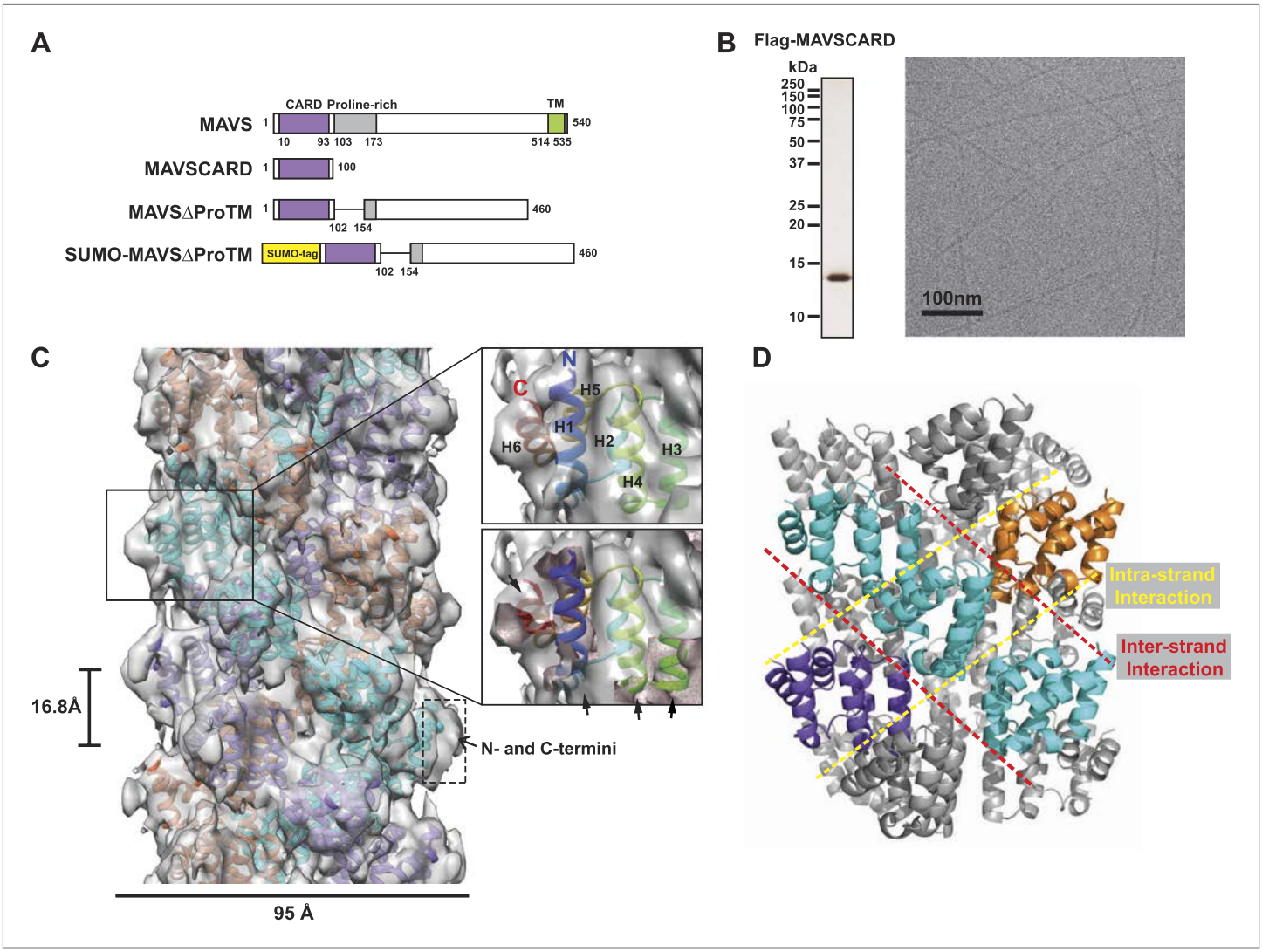

Figure 1. CryoEM reconstruction of MAVS CARD filaments. (**A**) Diagrams of the domain organization in MAVS and deletion mutants used in this study. (**B**) Flag-MAVS CARD purified from HEK293T cells analyzed by silver stained SDS-PAGE and cryoEM imaging. The cryoEM image is displayed in reversed contrast (protein in black) for better visualization. (**C**) Left: a side view of the final 3D reconstruction of MAVS CARD filament. The X-ray crystal structure model of the human MAVS CARD (PDB: 2VGQ) was docked into the cryoEM map. Three strands are colored differently. Right: the rod-like densities at the periphery of the cryoEM density map allowed positioning of H1, H4, H3 and H6 without modification (top; see ***Video 2***). When a front part of the density map was sectioned off with a clipping plane (red mesh), the H1 helix (blue) fitted into a rod-like density very well (bottom). (**D**) Pseudoatomic model of MAVS CARD filament. Dashed lines indicate the inter- (red) and intra-strand (yellow) interaction interfaces.

DOI: 10.7554/eLife.01489.003

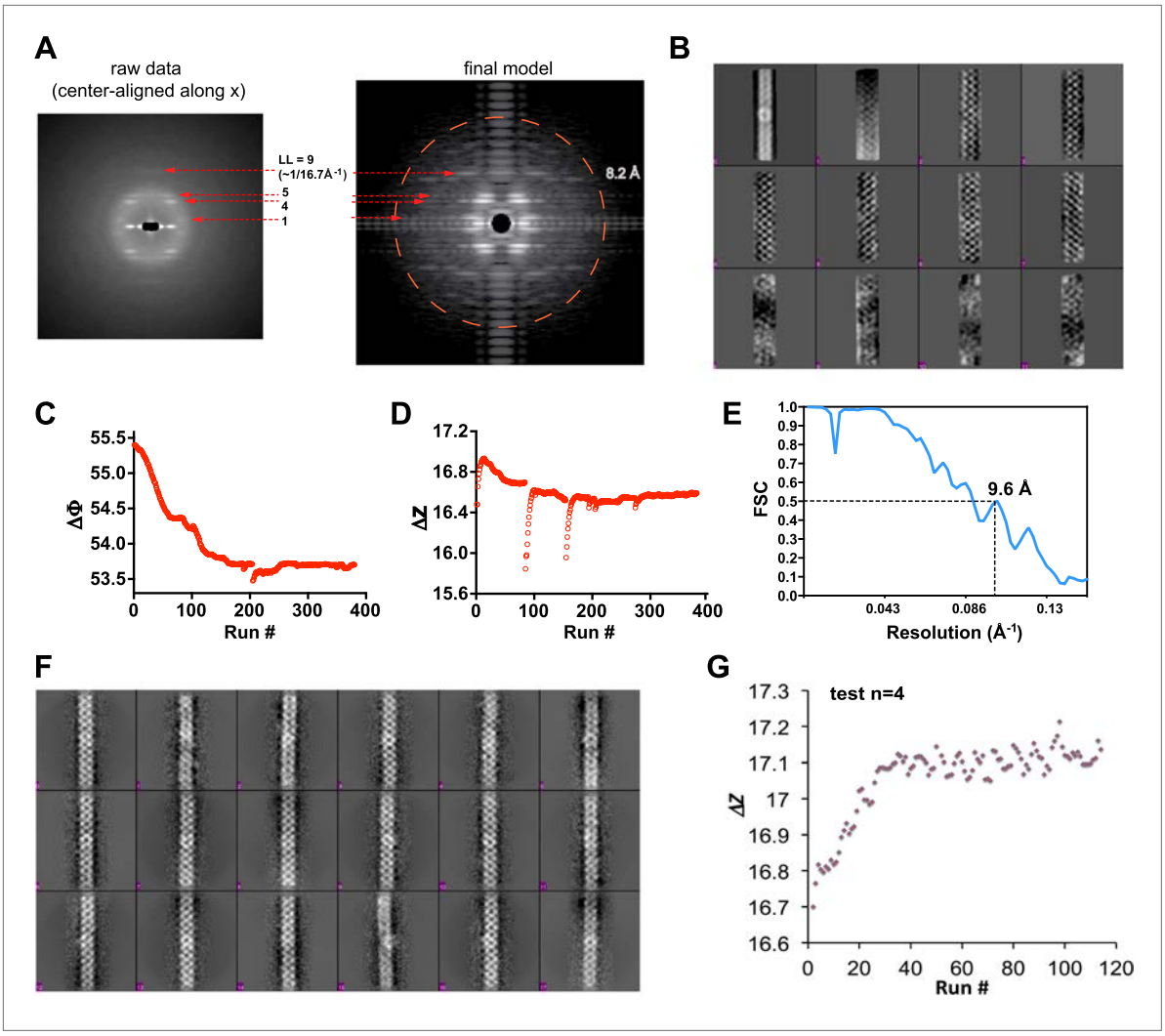

Figure 1—figure supplement 1. Processing of cryoEM images of the MAVS CARD filaments.

DOI: 10.7554/eLife.01489.004

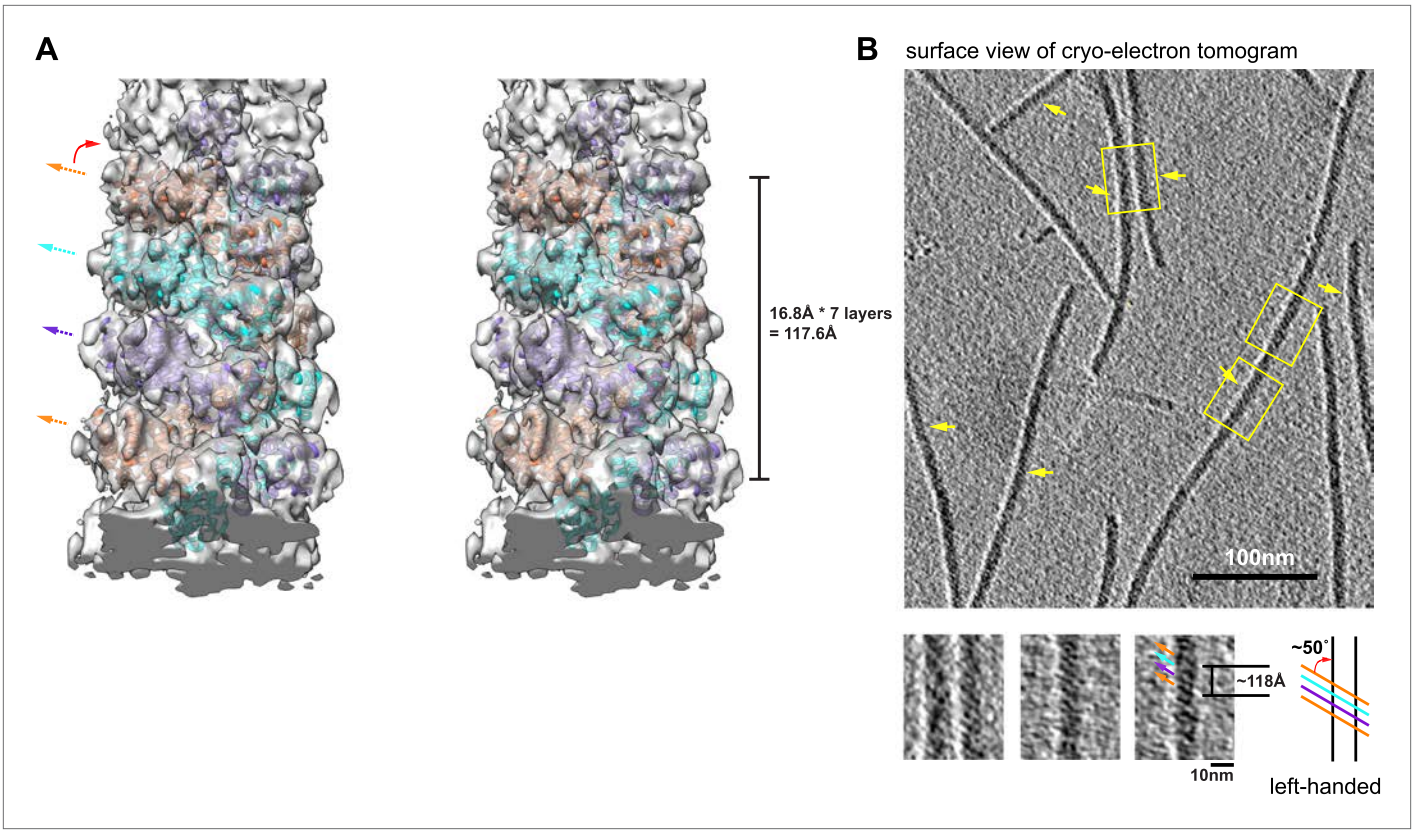

Figure 1—figure supplement 2. Structural model of MAVS CARD filaments and its chirality determination by cryo electron tomography (cryo-ET).
DOI: 10.7554/eLife.01489.005

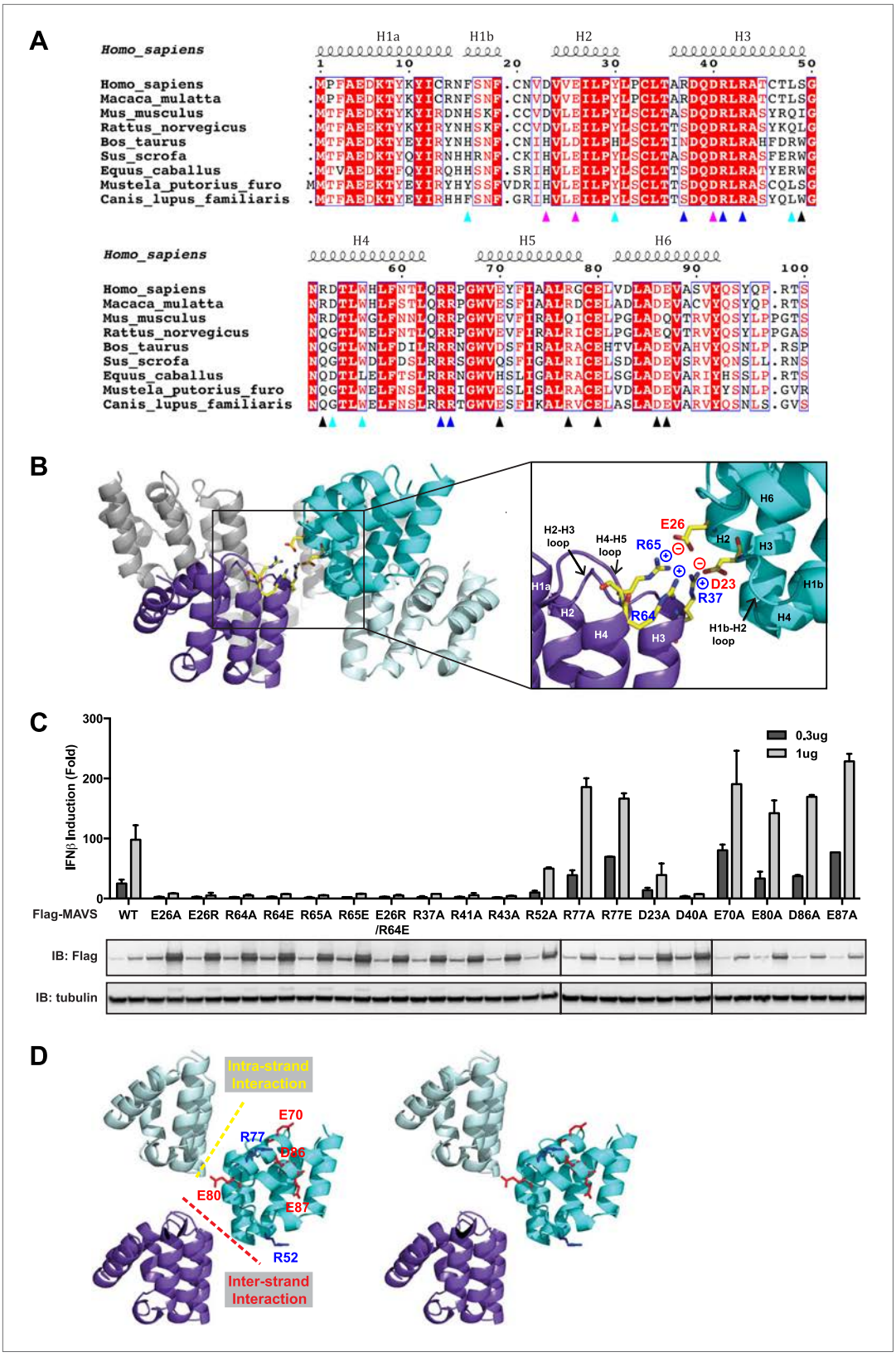

Figure 2. Charged residues are conserved at the inter-strand interface of MAVS CARD filament. (**A**) Sequence alignment of the MAVS CARD from 10 different species with the secondary structures based on the X-ray model of human MAVS CARD. The alignment was generated with ClustalW (http://www.ebi.ac.uk/clustalw/) and formatted

Figure 2. Continued on next page

Figure 2. Continued

using ESPript (http://espript.ibcp.fr/ESPript/ESPript/). The colored arrowheads mark the residues mutated in this study: pink, key negatively charged residues at the inter-strand interface; blue, key positively charged residues at the inter-strand interface; cyan, key residues at the intra-strand interface; black, residues showing normal activity when substituted with alanine. (**B**) MAVS CARD hexamer model with key residues at the inter-strand interface between two subunits (purple and cyan) shown as yellow sticks. The inset on the right side is an expanded view of these residues. The side chains of these residues (D23, E26, R37, R64 and R65) in the model were optimized by testing different rotamers in Coot. (**C**) Effects of mutating the residues at the inter-strand interface and other conserved charged residues on MAVS activity. Wild-type MAVS and CARD mutants at different positions were transiently expressed in HEK293T-IFNβ-luciferase reporter cells. Cells were lysed 24 hr later, and the MAVS signaling was tested by luciferase reporter assay in a dose-dependent manner. Western blot was done to monitor the expression level of the transfected MAVS proteins with α-tubulin as loading controls. (**D**) A stereo view of MAVS CARD model with the surface-exposed, conserved charged residues shown as sticks (blue, positively charged residues; red, negatively charged residues). Mutations of these surface residues, which are not involved in the inter-strand interactions, do not impair MAVS signaling.
DOI: 10.7554/eLife.01489.008

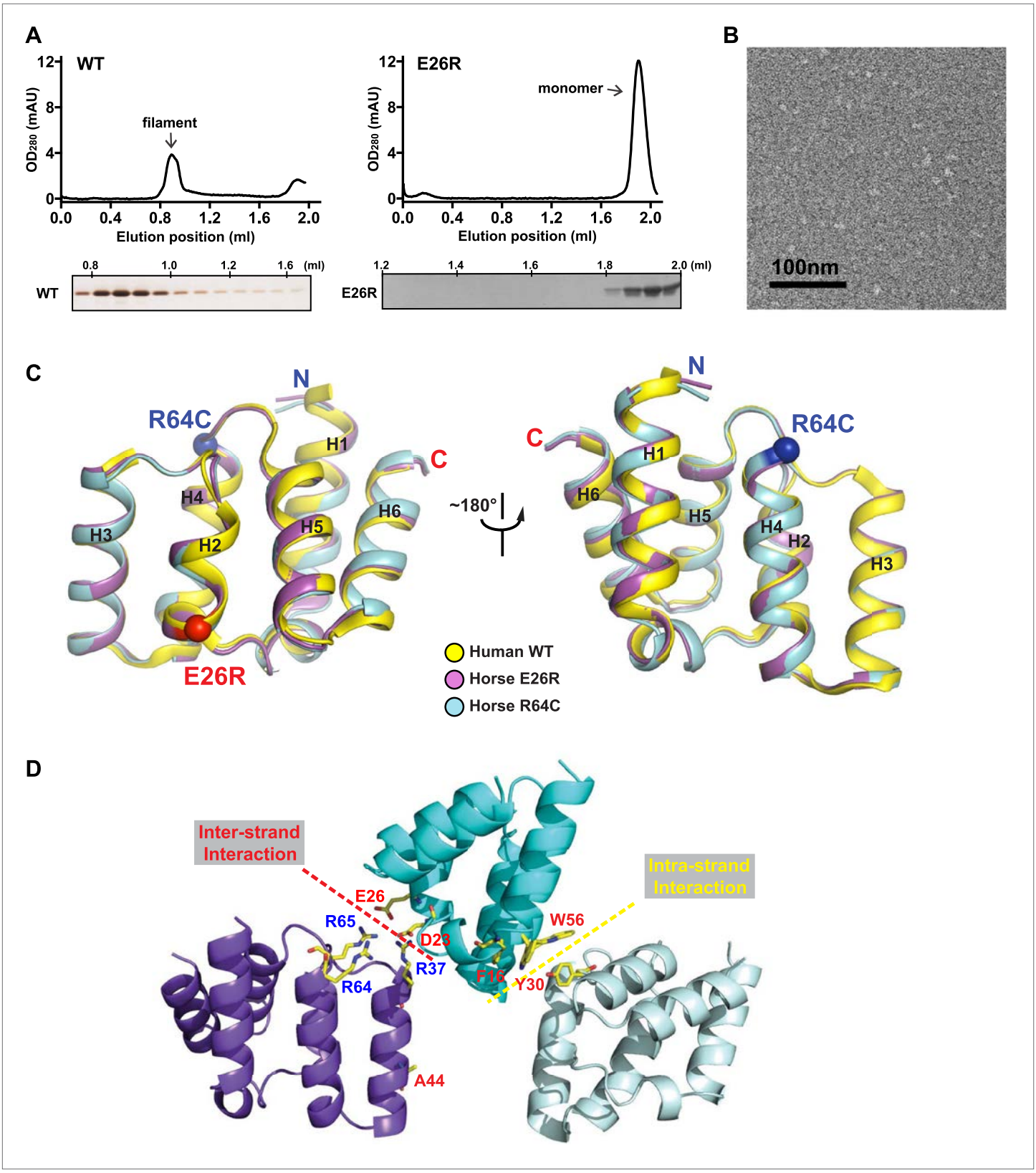

Figure 2—figure supplement 1. Mutations at the inter-strand interface disrupt MAVS CARD polymerization.

DOI: 10.7554/eLife.01489.009

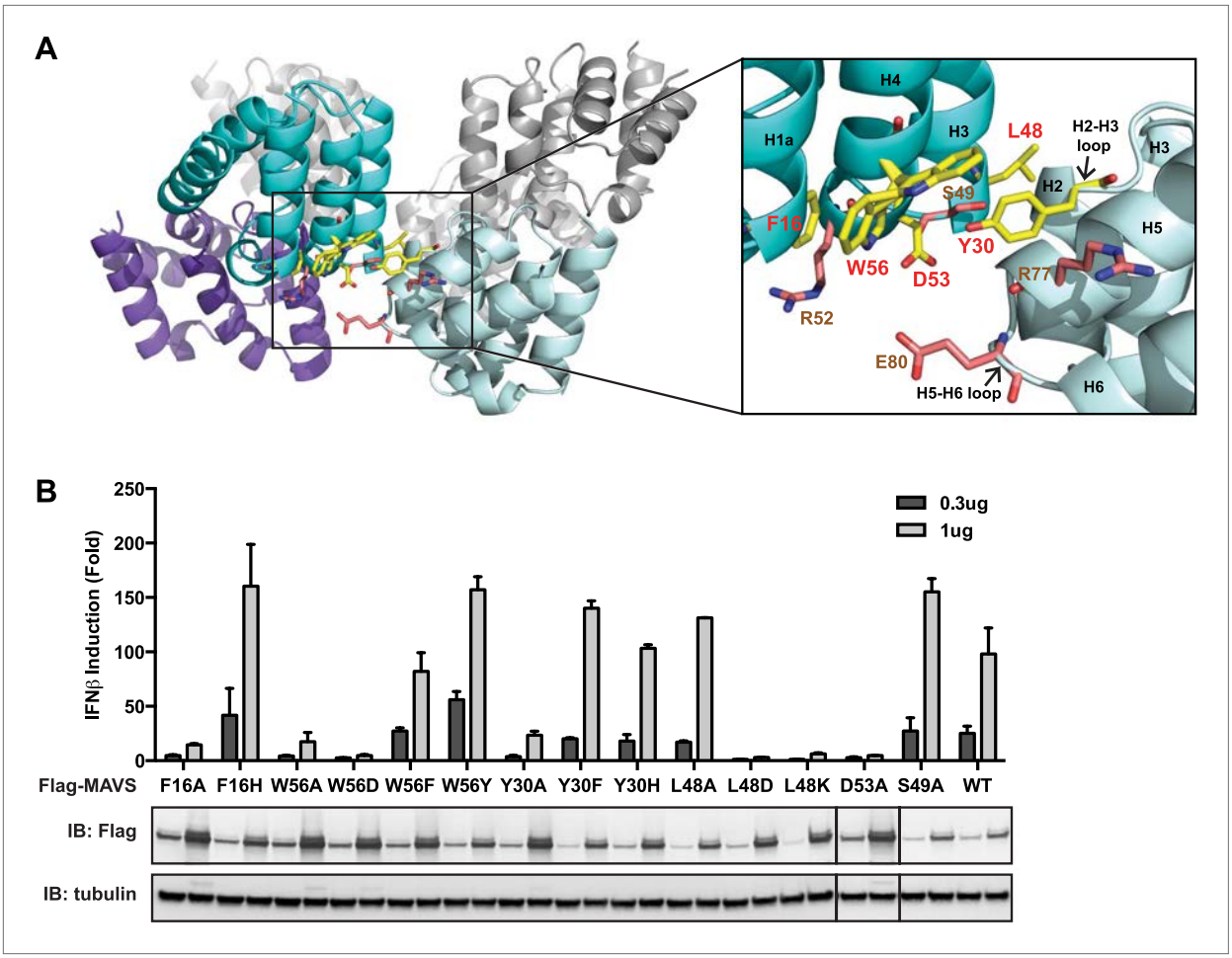

Figure 3. The intra-strand interface is mediated by hydrophobic interactions and hydrogen bonding. (**A**) MAVS CARD hexamer model with interacting residues at the intra-strand interface shown as yellow sticks. Residues that showed normal activity when substituted with alanine are displayed in brown. (**B**) MAVS proteins with point mutations at the intra-strand interface were tested for IFNβ induction and protein expression as in ***Figure 2C***.

DOI: 10.7554/eLife.01489.011

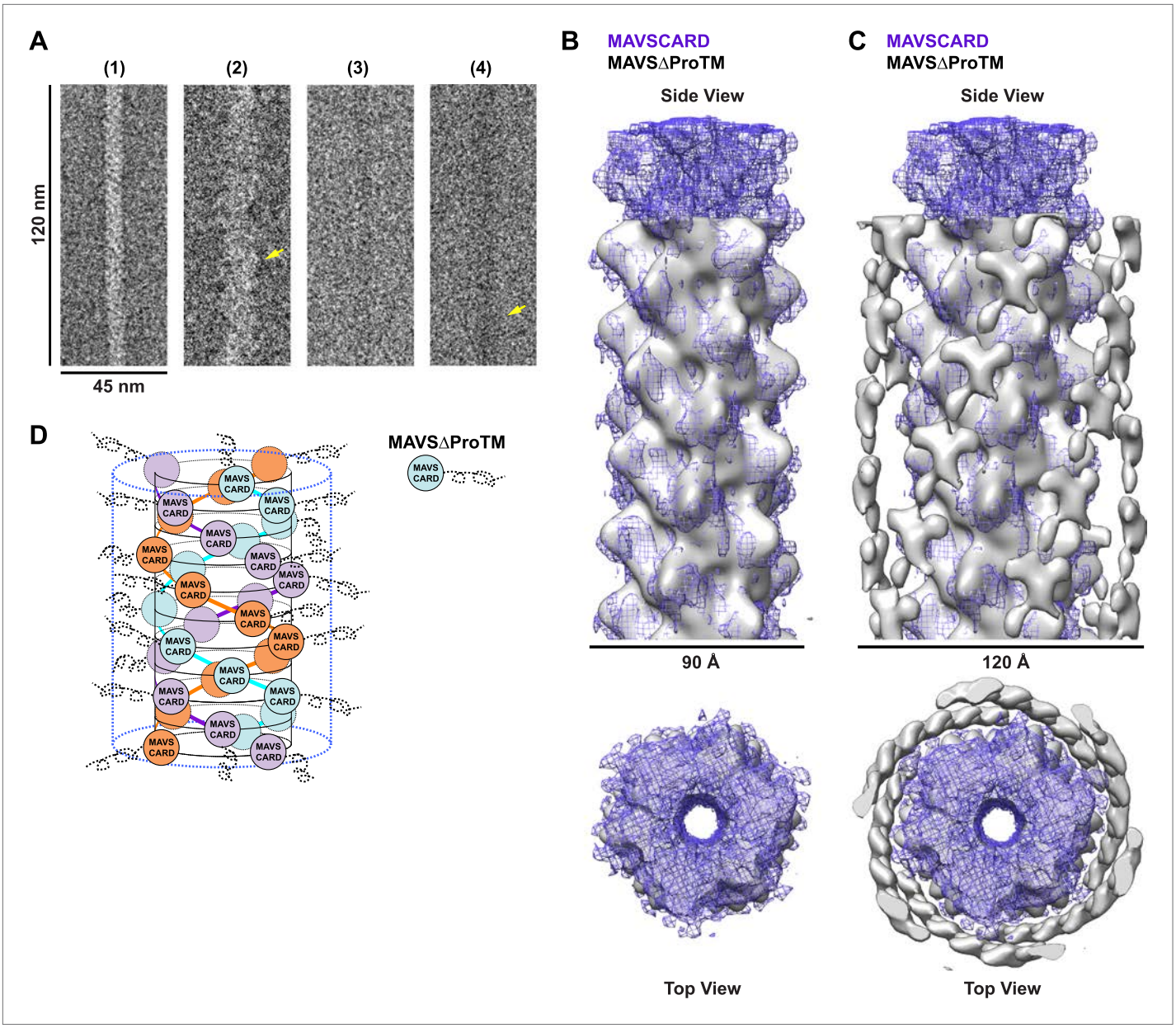

Figure 4. CARD filament is the organization center of the MAVS Filament. (**A**) Segments from negative-stain EM images of (1) Flag-MAVS CARD and (2) MAVSΔProTM and those from cryoEM images of (3) Flag-MAVS CARD and (4) MAVSΔProTM. For better visualization, protein is black in the cryoEM images. Yellow arrows point to the extra mass that made the MAVSΔProTM filaments larger in diameter. (**B**) Side and top views of the cryoEM reconstruction of MAVSΔProTM filament (gray, surface), which has the same helical symmetry as the MAVS CARD filament (purple, mesh). Only the middle 90 Å portion of the MAVSΔProTM map is shown. (**C**) Side and top views of the full MAVSΔProTM map (gray, surface) whose threshold was set at a proper level to overlap well with the CARD-only map (purple, mesh). A cylindrical sheet of extra density appeared at ~15 Å away from the central CARD filament. (**D**) Schematic view of the helical packing of MAVSΔProTM with the sequences C-terminal to the CARD shown as dashed coils.

DOI: 10.7554/eLife.01489.012

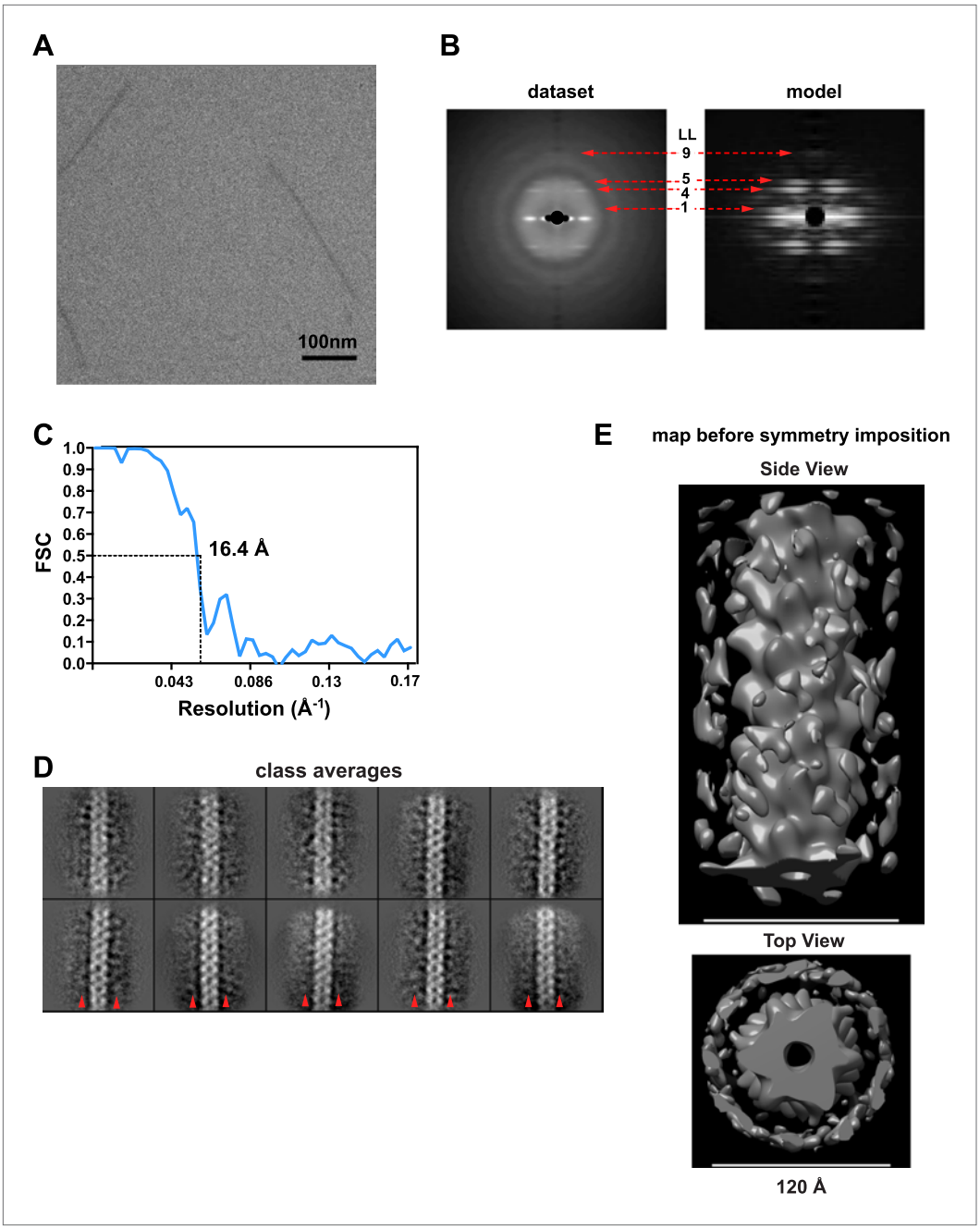

Figure 4—figure supplement 1. Image processing for the MAVSΔProTM filaments.

DOI: 10.7554/eLife.01489.013

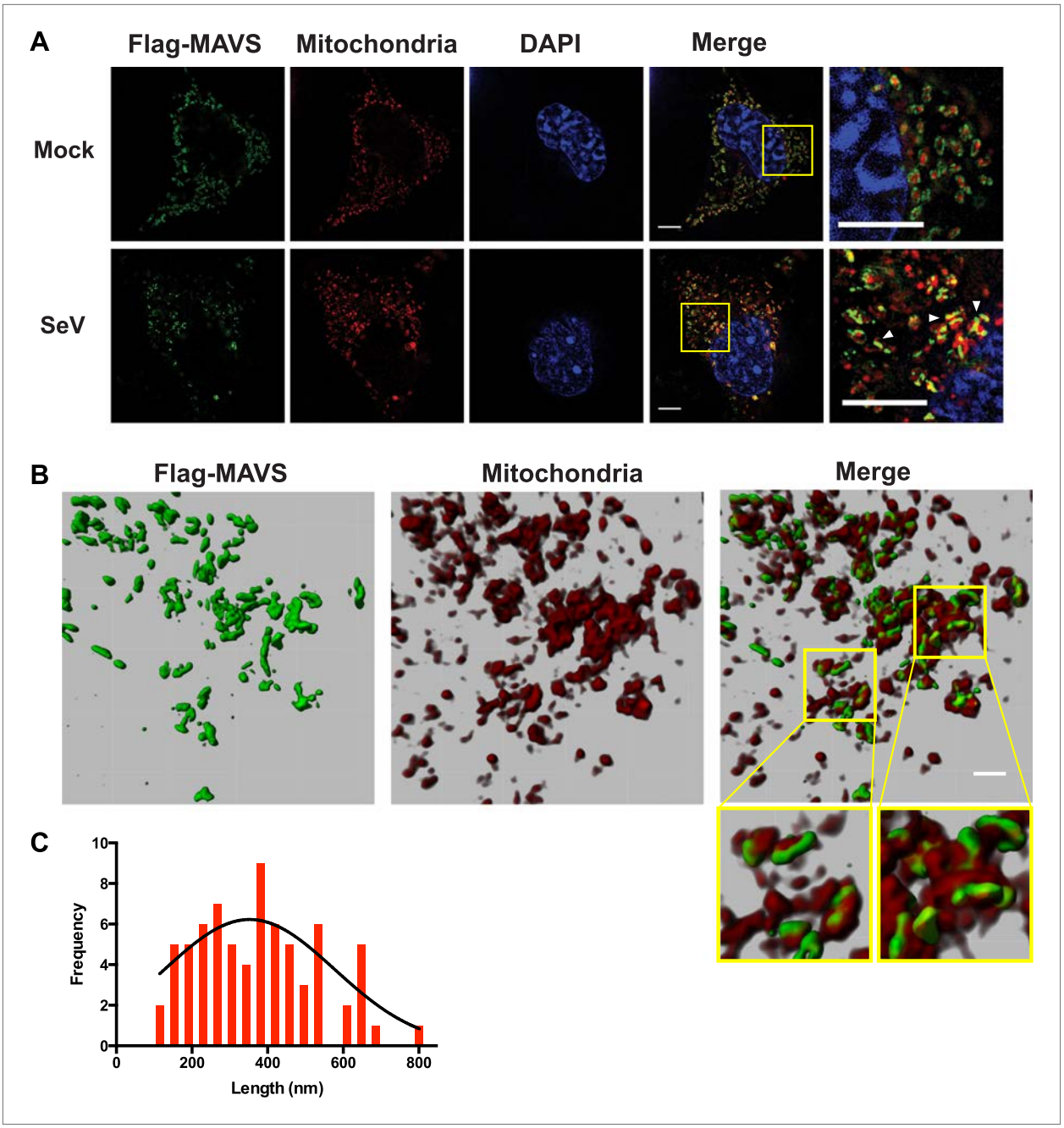

Figure 5. In virus-infected cells MAVS redistributes and forms rod-shaped puncta on the surface of mitochondria. (**A**) *Mavs*$^{-/-}$ MEF cells stably expressing Flag-tagged wild-type MAVS were mock-treated or infected with Sendai virus (SeV) for 12 hr and stained with MitoTracker (Mitochondria; red) and anti-Flag antibody (Flag-MAVS; green). Redistribution of MAVS among mitochondria was examined using SR-SIM. Expanded views of the areas within the yellow windows in the merged images were shown on the right. The SeV-infected cells contain bright foci of Flag-MAVS. The white arrowheads in the rightmost image of the bottom row highlight a few bright rod-shaped MAVS clusters. Scale bars, 5.0 μm. (**B**) 3D reconstruction of MAVS clusters (green) on the surface of mitochondria (red). Scale bar, 1.0 μm. The areas within the yellow windows in the merged image (right most) were expanded to show a few clusters that appear to bridge between mitochondrial membranes. (**C**) Histogram and Gaussian fit (black curve) of the length distribution that was measured from the SIM images of individual MAVS clusters as in panel **A** (SeV; N = 74) in virus-infected cells.

DOI: 10.7554/eLife.01489.014

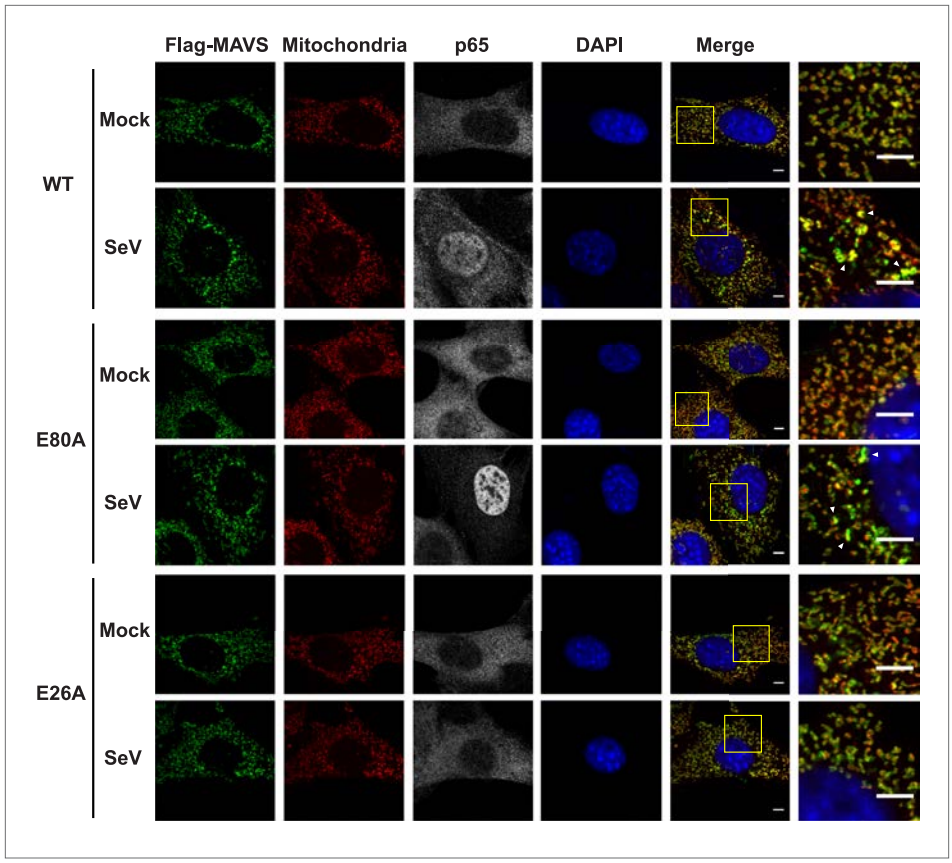

Figure 5—figure supplement 1. Mutations at the inter-strand interface that disrupt CARD polymerization abolish the SeV-induced redistribution of MAVS on mitochondria.

DOI: 10.7554/eLife.01489.015

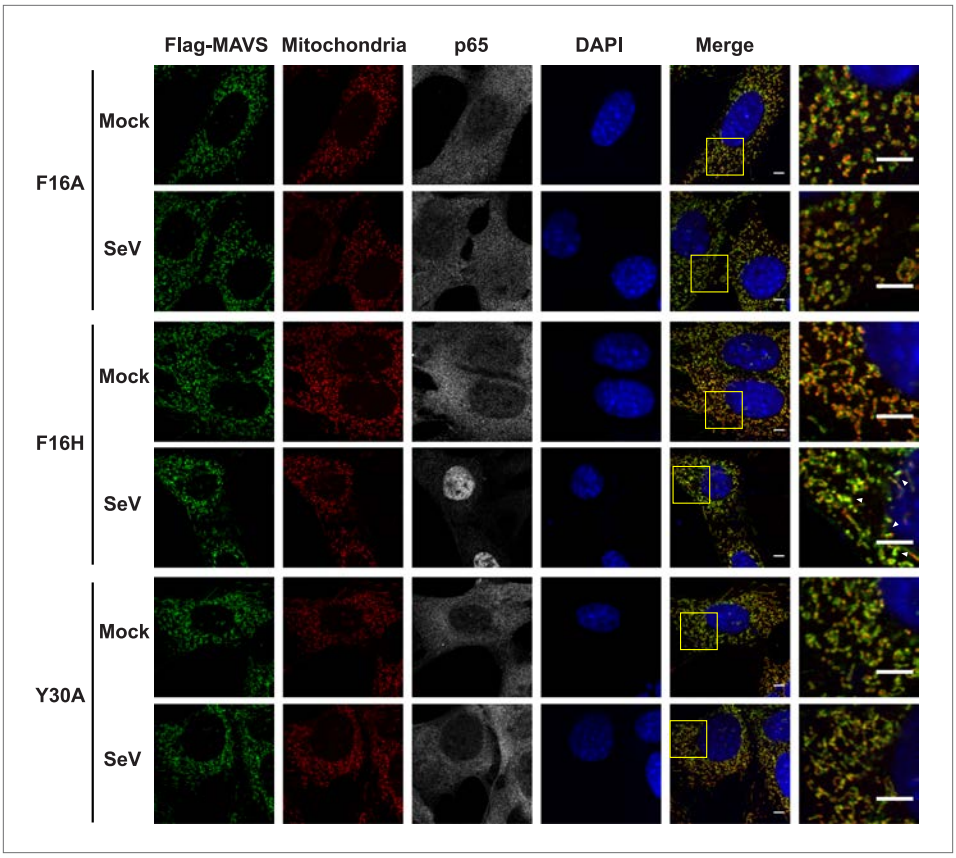

Figure 5—figure supplement 2. Mutations at the intra-strand interface that disrupt CARD polymerization abolish the SeV-induced redistribution of MAVS on mitochondria.

DOI: 10.7554/eLife.01489.016

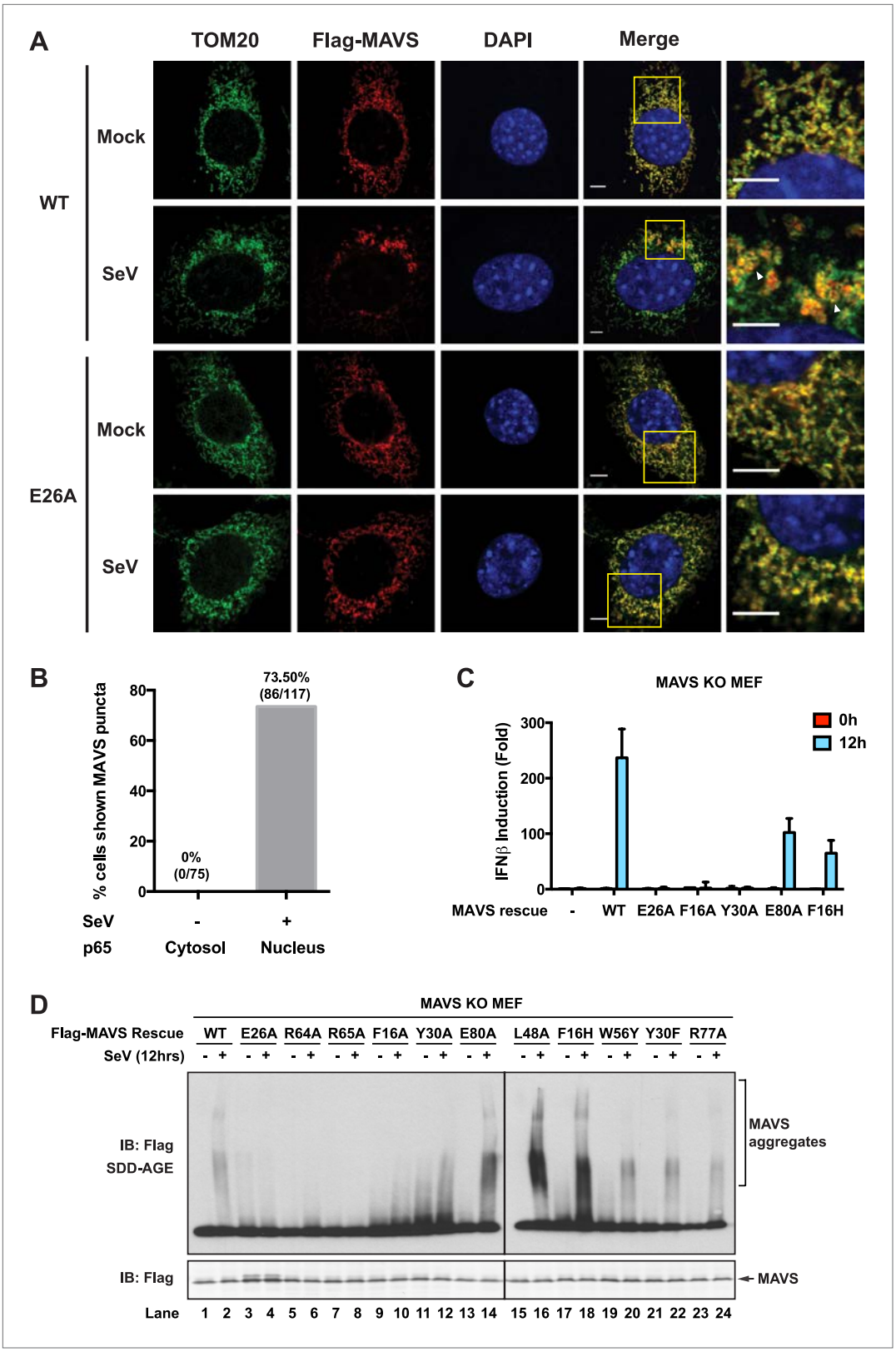

Figure 5—figure supplement 3. Strong correlations among MAVS puncta formation, MAVS signaling and MAVS CARD polymerization.

DOI: 10.7554/eLife.01489.017

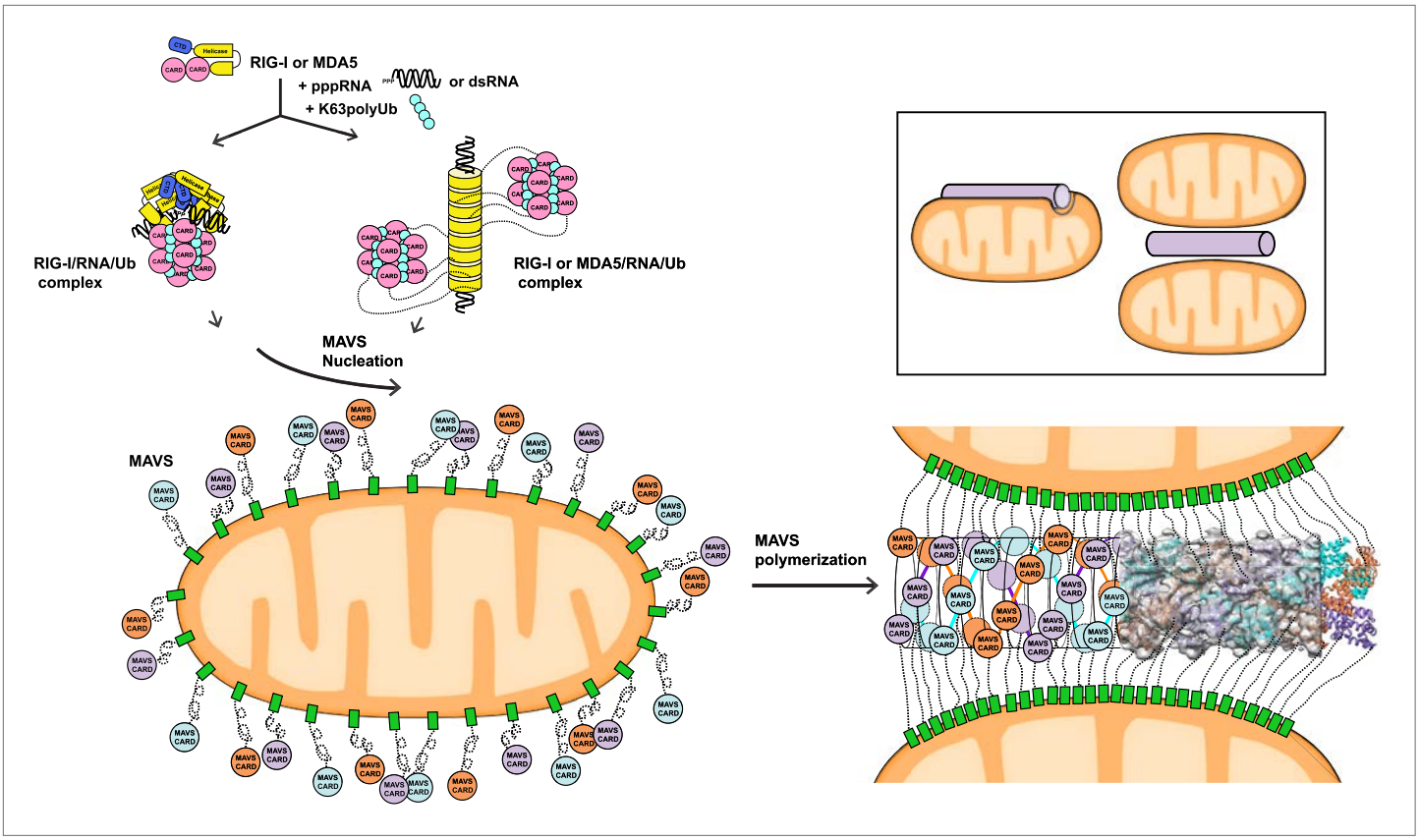

Figure 6. A working model for MAVS activation by RIG-I/RNA complexes. Detection of 5′-pppRNA by RIG-I or dsRNA by MDA5 or RIG-I triggers the formation of RIG-I (or MDA5)/RNA/polyUb complex. The CARD domains of individual complexes are poised properly to attract three MAVS CARD domains and support the nucleation of the filament. In the resting state, MAVS CARD is sequestered and has a low probability of forming polymers. The RIG-I (or MDA5)/RNA/polyUb complexes stabilize the MAVS CARDs in the exposed state and bring three copies together to initiate the filament formation. Once started, a short MAVS CARD filament promotes its own elongation by attracting more MAVS CARDs into the assembly. The filament can form on the surface of one mitochondrion or between two or more mitochondrial membranes. Inset, one or more mitochondria might be involved in MAVS filament formation.

DOI: 10.7554/eLife.01489.018